Analysis of Permanent Magnet Wind Turbine Dynamics During Wind Fluctuations

Maryam Bahramgiri[1], Ali Abedini[2], Alireza Siadatan[3]
1- Department of Electrical Engineering, West Tehran Branch Islamic Azad University, Tehran, Iran.
2- Electrical and Computer Engineering Department, Khaje Nasir Toosi University of Technology, Tehran, Iran.
3- Department of Electrical Engineering, West Tehran Branch Islamic Azad University, Tehran, Iran.

Received: February 2012 Revised: August 2012 Accepted: September 2012

ABSTRACT:
This paper analyzes the behavior of a Permanent Magnet Synchronous Generator (PMSG) wind turbine using the maximum power extraction (MPE) method in response to wind speed fluctuations. The behavior of the wind turbine in the frequency domain will be analyzed to have the wind turbine response in the frequency domain. By combining the wind speed frequency content and wind turbine frequency response, the frequency content of wind turbine output power fluctuation will be gained. A PMSG wind turbine system is simulated with real wind speed data in the PSIM software environment, and the results are compared with theoretical results for validation of the model.

KEYWORDS: Wind turbine, Wind Fluctuations, Permanent Magnet.

1. INTRODUCTION

Wind is ubiquitous. It is a natural source of energy. Two percent of wind energy is sufficient to power the world. The technology enhancement has caused feasible advanced wind turbines and with reasonable price.

Due to the world–wide concerns about the energy sustainability and the environmental issues related to traditional power plants, governments have provided incentives for a greater use of wind energy. Although wind energy sources offer environmental and in some cases economic benefits, their utilization in the electric power systems has been facing with many technical challenges. The main technical challenges include power quality, reliability, and protection [1-6].

Although wind is a free and abundant source of energy and hence, is attractive in terms of the cost and energy security, wind is in nature intermittent and its energy has a large range of variations. This causes significant technical challenges for a wind energy conversion system, particularly when compared with the conventional energy sources which have a controllable output power.

One of the major technical problems of wind conversion systems is the fluctuations of the output power. The power fluctuations can cause frequency deviations, which may lead to system instability, particularly in power networks with a high penetration of wind energy systems. Additionally, since the output power of wind conversion systems varies with time, they are usually considered as negative loads and not dispatchable sources like the conventional generation systems. As a result, a wind conversion system is not a controllable source of energy whose output power can be regulated based on the load demand.

On the other hand, the susceptibility of the power grid is a function of the frequency of the power fluctuations. Luo et al developrd a transfer function in [7] that demonstrates the susceptibility of the power network versus the power variation frequency. Based on to this transfer function, the fluctuations that occur between 0.08 to 0.5 Hz are more hazardous from stability point of view.

This paper is intended to discover the wind power oscillation spectrum so that suitable compensators are considered to maintain the stability of the grid. Since the frequency of the wind power oscillations is mainly dependent on wind speed oscillations and the dynamic of the wind turbine system, the wind speed behavior and the dynamics of the wind turbine system will be discussed extensively.

This paper is organized as follows. Section II discusses dynamic of each part of a wind turbine system. Section III the susceptibility of a power grid is obtained. In section IV, the behavior of wind is explained in the frequency domain. The maximum power extraction control method is explained in section V. The MPE method frequency response is explained in continue of section V. The wind speed spectrum and MPE frequency response are combined, and wind power fluctuations spectrum is gained. A PMSG wind turbine is simulated in PSIM, and the results are compared with the analytical method in section VI.

2. WIND TURBINE SYSTEM TOPOLOGY

The overall discussed wind turbine system is shown in Figure 1. This Figure shows the block diagram of a direct driven wind turbine. But the discussion of this paper is general and can be applied to other wind turbine systems. The goal of this paper is to find out the dynamic of the wind turbine such that when the wind speed variations are known then the output power variation of the system will be achieved. Most of the wind turbine systems consist of a turbine, generator and power electronic subsystems. The dynamic of wind turbine is the combination of the dynamic of each subsystem. In this paper the dynamic of each part is first obtained and then the overall dynamic of the wind turbine system is developed.

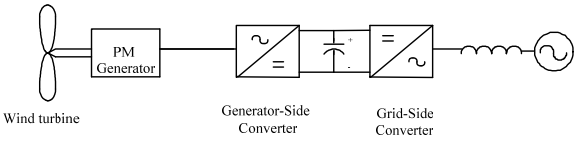

Fig. 1. The topology of the wind turbine system.

A. Wind turbine

Equations (1)-(4) describe the wind turbine model. Equation (1) shows the output power that can be extracted from the wind. The coefficients in (1) are given in (2)-(4) [8].

$$P = c(\beta,\lambda)\frac{\rho A}{2}v_{wind}^3 \tag{1}$$

$$c(\beta,\lambda) = c_1(\frac{c_2}{\lambda_2} - c_3\beta - c_4)e^{-\frac{c_5}{\lambda_2}} + c_6\lambda \tag{2}$$

$$\frac{1}{\lambda_2} = \frac{1}{\lambda + 0.08\beta} - \frac{0.035}{\beta^3 + 1} \tag{3}$$

$$\lambda = \frac{R\omega}{v_{wind}} \tag{4}$$

where $\rho = 1.2\ kg/m^3$ is the air density, A is the area swept by the turbine blades, λ is the Tip-Speed-Ratio (TSR) that is given by (4), β is the pitch angle, *c* is performance coefficient of the turbine given in (2), and ω is the generator angular velocity. c_1-c_6 are coefficients which are dependent on the structure of the wind turbine.

B. PMSG

Figure 2 shows the d and q axes and the flux direction of the PMSG. θ is the angel between the rotor *d*-axis and the stator axis. Equation (5) expresses the state space model of the PMSG used in this paper [7].

The following assumptions are also considered in modeling the PMSG.

There is no damper winding.

Saturation is negligible.

Eddy-current and hysteresis losses are ignored.

Power losses are considered constant.

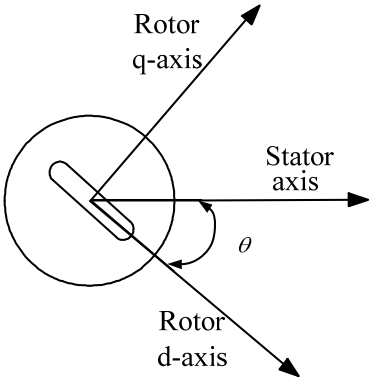

Fig. 2. *d-q* axis of a typical rotating machine.

$$\begin{bmatrix} i_{qs} \\ i_{ds} \\ \omega_s \end{bmatrix}^{\bullet} = \begin{bmatrix} \frac{R_s}{L_{qs}} & -\omega_s\frac{L_{ds}}{L_{qs}} & -\frac{\lambda_m}{L_{qs}} \\ \omega_s\frac{L_{qs}}{L_{ds}} & \frac{R_s}{L_{ds}} & 0 \\ -\frac{1.5P^2}{4J}\lambda_f & -\frac{1.5P^2}{4J}(L_{ds}-L_{qs})i_{qs} & -\frac{BP}{2J} \end{bmatrix} \begin{bmatrix} i_{qs} \\ i_{ds} \\ \omega_s \end{bmatrix} + \begin{bmatrix} \frac{-1}{L_{qs}} & 0 & 0 \\ 0 & \frac{-1}{L_{ds}} & 0 \\ 0 & 0 & \frac{P}{2J} \end{bmatrix} \begin{bmatrix} v_{qs} \\ v_{ds} \\ T_m \end{bmatrix} \tag{5}$$

where R_s is the stator resistance, L_{ds} and L_{qs} are the d-q axis inductances, P is number of poles, J is the rotor inertia, v_{ds} and v_{qs} are terminal voltage, i_{ds} and i_{qs} are d and q components of terminal currents, T_m is the input mechanical torque of the wind turbine, λ_m is the magnitude of the flux produced by the permanent magnet.

ω_s is the electrical rotor speed and is given by (6).

$$\omega_s = \frac{P}{2}\omega_m \tag{6}$$

ω_m is the mechanical rotor speed.

C. Main Converter

Figure 3 shows a detailed representation of the back-to-back converter of Figure 1. It includes a converter at the generator side which is connected to the dc link of a voltage-sourced converter at the grid side. The generator-side converter rectifies the generator output voltage to dc voltage which is then converted to ac three phase voltage by the grid-side

converter.

Figure 4 shows a dynamic model of the wind conversion system of Figure 3 including that of the back-to-back converter of Figure 3. The model includes *dq* representations of the PMSM and the energy storage that were presented in Sections 4 (a) and (b). Details related to development of the dynamic model of Figure 4 are presented in [10].

Based on the model of Figure 5, the wind conversion system can be represented by the following mathematical equations.

$$\begin{bmatrix} v_{dg} \\ 0 \end{bmatrix} = \begin{bmatrix} R_{sg} + L_{dg}D & -\omega_g L_{qg} \\ \omega_g L_{dg} & R_{sg} + L_{qg}D \end{bmatrix} \begin{bmatrix} i_{dg} \\ i_{qg} \end{bmatrix} + \begin{bmatrix} \frac{1}{2} A_{mg} v_{dc} \cos(\alpha_{mg} - \alpha_g) \\ \frac{1}{2} A_{mg} v_{dc} \sin(\alpha_{mg} - \alpha_g) \end{bmatrix} \quad (7)$$

$$\begin{bmatrix} v_{d\infty} \\ 0 \end{bmatrix} = \begin{bmatrix} -R_{sn} - L_{dn}D & \omega_n L_{qn} \\ -\omega_n L_{dn} & -R_{sn} - L_{qn}D \end{bmatrix} \begin{bmatrix} i_{dn} \\ i_{qn} \end{bmatrix} + \begin{bmatrix} \frac{1}{2} A_{mn} v_{dc} \cos(\alpha_{mn} - \alpha_n) \\ \frac{1}{2} A_{mn} v_{dc} \sin(\alpha_{mn} - \alpha_n) \end{bmatrix} \quad (8)$$

$$\frac{dv_{dc}}{dt} = 1/C(i_{dcg} - i_{dcn} - i_{sm}) = 1/C(\frac{p_g}{v_{dc}} - \frac{p_n}{v_{dc}} - i_{sm}) \quad (9)$$

i_{sm} represents the energy storage current and D denotes $\frac{d}{dt}$.

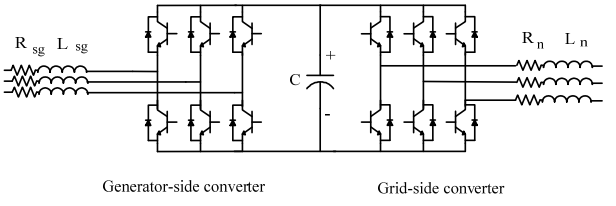

Fig. 3. The main converter system.

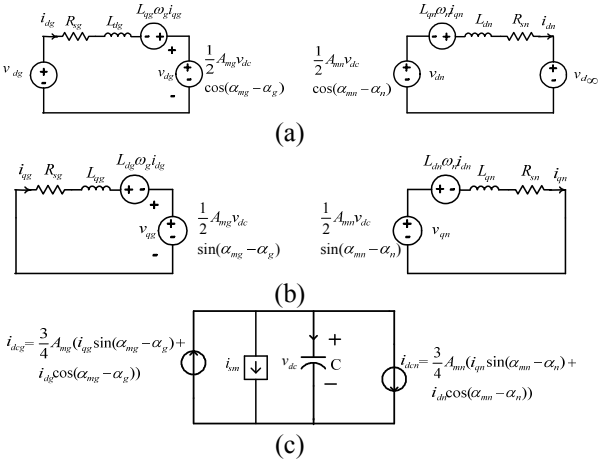

Fig. 4. Dynamic model of the wind conversion system of Figure 3.

3. GRID SUSCEPTIBILITY

Power fluctuation causes frequency deviation. The amount of frequency deviation caused by power fluctuation depends on the type and size of the grid. Here, an example of a typical grid consisting of three thermal plants is explained. The configuration of the grid is shown in Figure 5.

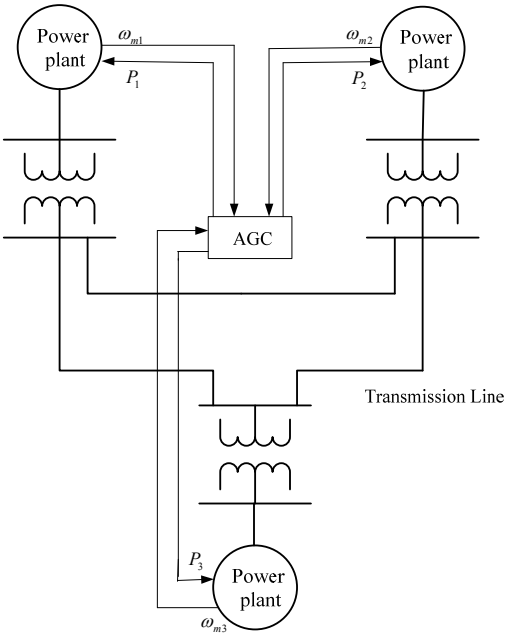

Fig. 5. The configuration of a typical power grid.

The objective of this evaluation is to find how power fluctuation $P(f)$ at frequency f_o affects the frequency of the system. The transfer function $G(f_o)$ is defined in 10.

$$G(f_o) = \frac{\Delta f_o}{\Delta P(f_o)} \quad (10)$$

The overall transfer function is:

$$\frac{1}{G(f_o)} = \frac{1}{\sum_{i=1}^{3} G_i(f_o)} \quad (11)$$

where $G_i(f_o)$ is the susceptibility of each power plant.

Usually each plant is equipped with a speed governor and Automatic Generation Control (AGC). Figures 6 and 7 show the block diagram of a speed governor and AGC system.

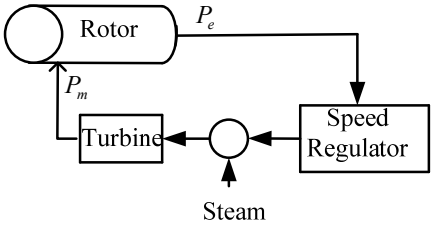

Fig. 6. Speed control loop for a thermal plant.

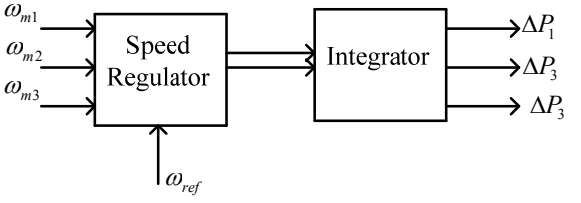

Fig. 7. The block diagram of the AGC.

Dynamic of a thermal plant without speed governor can be obtained as follows:

$$2H\frac{d\Delta\omega_r}{dt}=\frac{\Delta P_e}{\omega_0} \tag{12}$$

H is the inertia constant of the turbine. The dynamic of the system is derived by taking the Laplace Transformer of the equation.

$$G(s)=\frac{\Delta P_e}{\omega_0}=\frac{1}{2Hs\omega_0} \tag{13}$$

The bode plot of this transfer function is shown in Figure 8. As shown, the high frequency power fluctuation is filtered.

Figure 7 shows the dynamic of a system equipped with the speed governor against power fluctuation. Based on this plot, the low frequency power fluctuation cannot be smoothed by governor control system. This is due to the disability of the steam valve to open infinitely. It means after the value is completely open we can't increase the steam going to the turbine.

The third graph shows the dynamic of a power plant with governor and AGC control. As shown, having an AGC causes the graph converges to zero at very low frequency.

By combining all three plants in Figure 9 the dynamic of the power grid can be obtained. Figure 9 shows the dynamic of each individual power plant and the defined system in Figure 5 based on the (13). This Figure shows the susceptibility of the grid on the hand. This means power fluctuation in region B can adverse the stability of the system more than region A and C.

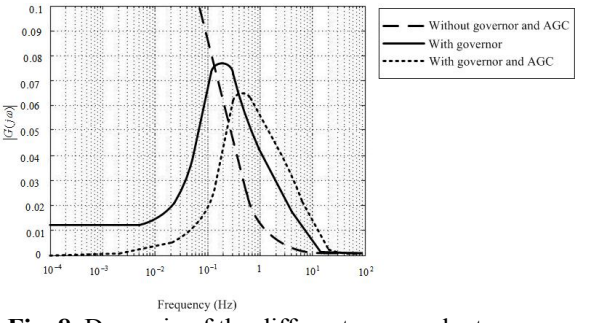

Fig. 8. Dynamic of the different power plants versus power fluctuation frequency.

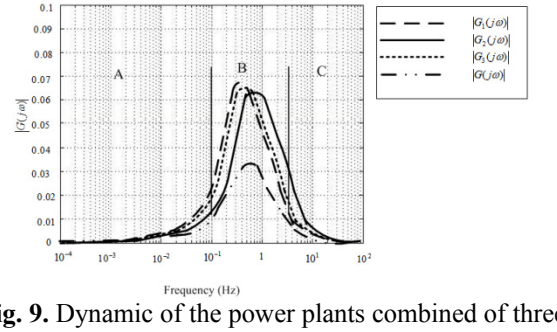

Fig. 9. Dynamic of the power plants combined of three power plants versus power fluctuation frequency.

4. WIND SPEED MODEL

Since the frequency of power variation depends mainly on wind frequency oscillation, it is important to find out a model associated with wind speed variation that can describe how wind speed variation is spread out in frequency domain. Different models have been developed to demonstrate the wind speed behavior [14-16]. Equation (14) presents the wind model presented by Rawn et al in [17].

$$v_w(t)=V_0+\sum_{i=1}^{n}A_i\cos(\omega_i t+\phi_i) \tag{14}$$

where V_0 is the average wind speed, A_i is the amplitude of the wind speed component at ω_i, ϕ is the phase of the wind speed component at ω_i and n is the number of components. ω_i is a random variable that has *Von Karman* distribution described by following equation.

$$S_{vv}(\omega_i)=\frac{0.475\sigma^2(L/V_0)}{[1+(\omega_i L/V_0)^2]^{5/6}} \tag{15}$$

L shows the roughness of the area around the wind turbine and σ is the standard deviation of the wind speed distribution. S is an empirical function that is obtained by interpolating the field data. A_i is chosen so that the wind power is equal to the real data. Equation (3) provides a rough estimation for A_i.

$$A_i(\omega_i)=\sqrt{(S_{vv}(\omega_i)+S_{vv}(\omega_{i+1}))(\omega_{i+1}-\omega_i)} \tag{16}$$

Figure 10. shows a typical wind speed data. The

frequency spectrum of typical wind speed variations is shown in Figure 11. The dominant frequency components are located in region A. The variation frequencies located in region B also includes considerable magnitudes. Variations are almost negligible in region C.

Not all the wind speed variations are directly translated into output turbine power variations. The large inertia of wind turbines acts as a low pass filter and smoothes the output power to some extent. The high frequency components in region C are mitigated at the output power by large time constant of the mechanical system.

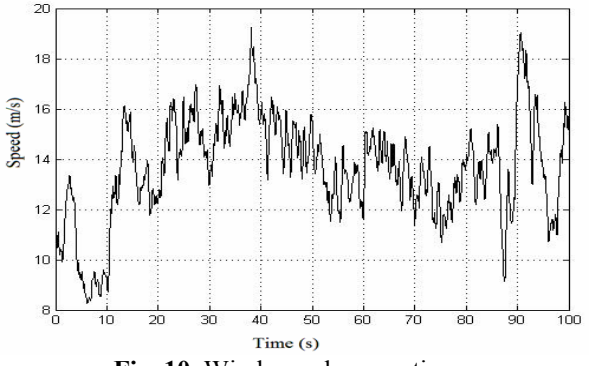

Fig. 10. Wind speed versus time.

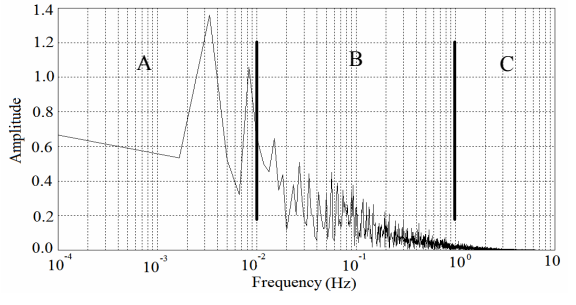

Fig. 11. Wind speed variations in frequency domain.

5. WIND TURBINE MODEL

In section IV, the wind speed spectrum was discussed. The power fluctuations are divided in three areas A, B and C. The power oscillations in region C are insignificant and negligible, while the power fluctuations in area A are the most. As mentioned in section IV, the wind turbine system acts as a low pass filter due to its large inertia. Therefore, the power fluctuations will have different spectrum after passing through wind turbine system. To find out the spectrum of wind turbine output power, the dynamic of the wind turbine must be developed. Since most of the wind turbines use maximum power extraction method, in this section the dynamic of the wind turbine will be studied by developing its transfer function when it uses MPE algorithm.

Since wind turbine adds dynamics to power conversion from wind to electricity, the power spectral density of a wind turbine is different from that of the wind, expressed in equation (14). Equation (17) shows the spectral density of the output power, considering a linear transfer function for wind turbine system.

$$S_P = \left|H(\omega)\right|^2 \left|A_\omega\right| \tag{17}$$

where A_w is given in (16) and $H(\omega)$ is the transfer function of the wind turbine, which also depends on the utilized control technique [6]. In this section, the transfer function of the wind turbine system is first obtained when the maximum power extraction method is applied to the wind turbine.

Wind energy is converted into kinetic energy and electrical energy as follows:

$$\Delta P_w = J\omega_{t0}\frac{d\Delta\omega_t}{dt} + \Delta P_e \tag{18}$$

ΔP_w and ΔP_e show the variations in wind power and electrical power and ω_{t0} denotes the initial wind turbine speed. Equation (1) shows the relationship among wind turbine output power, wind speed and wind turbine specifications. Wind turbine output power is mainly dependent to wind speed. Using (1), the following equations are achieved:

$$\Delta P_w = P_{w0}\frac{c'_{p_0}}{c_{p_0}}\Delta\lambda + 3P_{w0}\frac{\Delta v_w}{v_0} \tag{19}$$

$$\Delta\overline{P}_w = \lambda_0\frac{c'_{p_0}}{c_{p0}}(\Delta\overline{\omega}_t - \Delta\overline{v}_w) + 3\Delta\overline{v}_w \tag{20}$$

where $\Delta\overline{f} = \Delta f / f_0$ when f is P_w, v_w, and ω_t. c'_p is the derivative of c_p.

$$\Delta\overline{P}_e = (\frac{\partial P_w}{\partial\omega_t})(\frac{\omega_{t0}}{P_{e0}})\Delta\overline{v}_w \tag{21}$$

$\partial P_e / \partial\omega_t$ can be obtained from the control technique [6]. In MPE algorithm, the graph is shown in Figure 13. This parameter is called g. P_{e0} is also equaled to P_{w0} in the steady state.

By substituting (20) and (21) in (18), we have:

$$\lambda_0\frac{c'_{p_0}}{c_{p0}}(\Delta\overline{\omega}_t - \Delta\overline{v}_w) + 3\Delta\overline{v}_w = J\omega_{t0}\frac{d\Delta\omega_t}{dt} + g_0(\frac{\omega_{t0}}{P_{w0}})\Delta\overline{v}_w \tag{22}$$

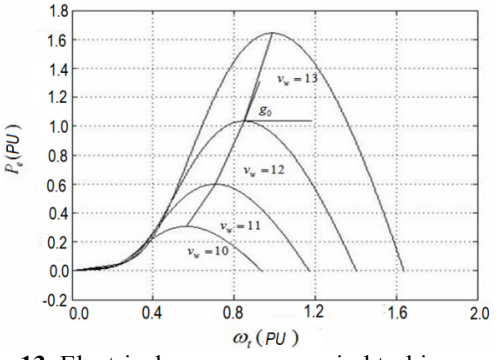

Fig. 13. Electrical power versus wind turbine speed.

By applying Laplace transform, (23) is derived.

$$\frac{\Delta\bar{\omega}_t(s)}{\Delta\bar{v}_w(s)} = \frac{3-\lambda_0(\frac{c'_{p_0}}{c_{p0}})}{\tau_0 s-\lambda_0(\frac{c'_{p_0}}{c_{p0}})+g_0(\frac{\omega_{t0}}{P_{w0}})} \quad (23)$$

where $\tau_0 = J\frac{\omega_{t0}^2}{P_{w0}}$.

Combining (21) in (23), the transfer function is achieved as follows.

$$\frac{\Delta\bar{P}_e(s)}{\Delta\bar{v}_w(s)} = \frac{3-\lambda_0(\frac{c'_{p_0}}{c_{p0}})g_0(\frac{\omega_{t0}}{P_{w0}})}{\tau_0 s-\lambda_0(\frac{c'_{p_0}}{c_{p0}})+g_0(\frac{\omega_{t0}}{P_{w0}})} \quad (24)$$

The magnitude of the transfer function of a typical system is depicted in Figure 14.

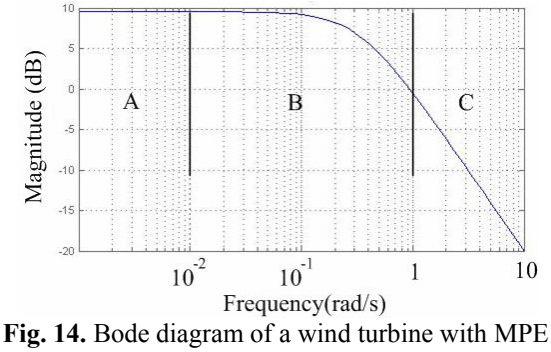

Fig. 14. Bode diagram of a wind turbine with MPE algorithm.

As shown, the wind turbine behaves very much like a low pass filter. The power fluctuation in region A is passed fully to the power grid, while those of region B and C will be attenuated.

6. SIMULATION RESULTS

In order to verify the theoretical results obtained from previous section, a PMSG wind turbine system of Figure 15 is implemented in PSIM software. And MPE method is applied. The wind turbine system parameters are given in Table 1. The wind speed data is shown in Figure 10. The wind speed spectrum is shown in Figure 11. The generator side converter determines the wind turbine speed to extract the maximum power and the grid side converter regulates the voltage of dc link and the amount of the reactive power required to deliver to the grid. This system is used space vector PWM technique for switching. And there are PI controllers to reduce the steady state errors of the system. The output power of the wind turbine is shown in Figure 16. The frequency content of the output power is given in Figure 17. As shown, the wind turbine output power oscillations are mostly in Area A. And the oscillations in Area B are attenuated compared to wind oscillation shown in Figure 11.

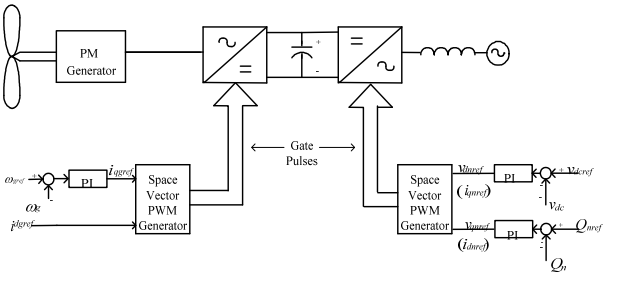

Fig. 15. The structure of the wind turbine system using a PMSG.

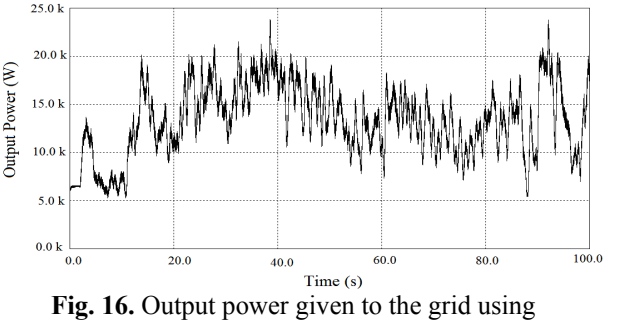

Fig. 16. Output power given to the grid using maximum extraction algorithm.

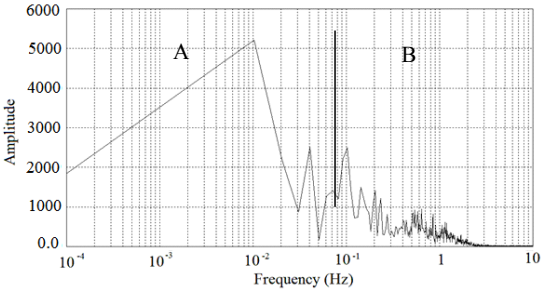

Fig. 17. Frequency content of power fluctuation.

Table 1: Parameters of the system of Fig. 15.

R_{sg}	0.0918 (Ω)	
L_{dg}	0.00195 (H)	Unsaturated
L_{qg}	0.00195 (H)	
R_{sn}	0.025 (Ω)	
L_{dn}	0.0007 (H)	
L_{qn}	0.0007 (H)	
λ_m	0.19 (V.s)	
P	10 kW	
J	0.1 kgm^2	
B	0.001 Ns/rad	
I_n	10	Grid-side converter controller integral gain
P_n	1	Grid-side converter controller proportional gain
I_{Gd}	2000	Generator-side converter controller integral gain (d axis)
P_{Gd}	100	Generator-side converter controller proportional gain (d axis)
I_{Gq}	2000	Generator-side converter controller integral gain (q axis)
P_{Gq}	100	Generator-side converter controller proportional gain (q axis)

7. CONCLUSION

In this paper the behavior of wind based on its model in frequency domain was discussed. The different components of a PMSG wind turbine are modeled. Due to nature of mechanical component the dynamic of a wind turbine is dominated by mechanical components. The wind turbine dynamic is developed based on its transfer function. The gained dynamic is used to analyze the wind turbine behavior in response to wind speed fluctuation. A PMSG wind turbine is simulated with real wind speed data and the output power is shown in frequency domain for comparison with wind speed spectrum. The simulation results verify the mathematical method. Therefore, wind turbine systems acts like a low pas filter. Low frequency power fluctuations (<0.1 Hz) will pass from wind turbine while high frequency power oscillations (>0.1 Hz) will be attenuated.

8. ACKNOWLEGMENT

This paper was supported by a grant from West Tehran Branch, Islamic Azad University.

REFERENCES

[1] C. Abbey and G. Joos, **"Supercapacitor Energy Storage for Wind Energy Applications,"** *IEEE Trans. Industry Applications*, vol. 43, no. 3, pp. 769 – 776, May-June 2007.

[2] T. Kinjo, T. Senjyu, N. Urasaki and H. Fujita, **"Terminal-voltage and output-power regulation of wind-turbine generator by series and parallel compensation using SMES,"** *IEEE Proceedings-Generation, Transmission and Distribution,* vol. 153, no 3, pp. 276 – 282, May 2006,.

[3] R. Cardenas, R. Pena, J. Clare and G. Asher, **"Power smoothing in a variable speed wind-diesel system,"** *in Proc.34th Annual IEEE Power Electronics Specialist Conference,* June 2003, pp. 754-759.

[4] C. Abbey and G. Joos, **"Attenuation of Wind Power Fluctuations in Wind Turbine Generators using a DC Bus Capacitor Based Filtering Control Scheme,"** *in Proc. 41stIEEE Industry Applications Annual Meeting*, vol. 1, 2006, pp. 216-221.

[5] L. Ran, J.R. Bumby and P.J. Tavner, **"Use of Turbine Inertia for Power Smoothing of Wind Turbines with a DFIG,"** *in Proc. 11st IEEE International Conference on power quality*, 2004, pp. 106-111.

[6] C. Luo, H. Banakar, B. Shen and B. T. Ooi, **"Strategies to Smooth Wind Power Fluctuations of Wind Turbine Generator,"** *IEEE Trans. Energy Convers.*, vol. 22, no. 2, pp. 341 - 349**,** June 2007.

[7] C. Luo, H. G. Far, H. Banakar, P.K. Keung and B. T. Ooi, **"Estimation of Wind Penetration as Limited by Frequency Deviation,"** *IEEE Trans. Energy Conversion.*, vol. 22, no. 3, pp. 783 – 791, Sept. 2007.

[8] A. Abedini and H. Nikkhajoee, **"Dynamic model and control of a wind-turbine generator with energy storage,"** *IET Trans. Renewable Power Generation.,* vol. 5, no. 1, pp. 67 – 78, 2011.

[9] C. Luo and B. T. Ooi, **"Frequency Deviation of Thermal Power Plants Due to Wind Farms,"** *IEEE Trans. Energy Convers.*, vol. 21, no. 3, pp. 708 – 716, Sept. 2006.

[10] T. Ackermann, **Wind Power in Power Systems,** John Wiley & Sons, 2005.

[11] M. Jelavic, N. Peric and S. Car, **"Estimation of wind turbulence model parameters,"** *ICCA International Conference on Control and Automation*, vol. 1, June 2005, pp. 89-94.

[12] R. Karki and Po Hu, **"Wind power simulation model for reliability evaluation,"** *Canadian Conference on Electrical and Computer Engineering*, May 2005, pp. 541-544.

[13] B.G. Rawn, P.W. Lehn and M. Maggiore, **"Control Methodology to Mitigate the Grid Impact of Wind Turbines,"** *IEEE Transaction on Energy Conversion*, vol. 22, no.2, pp. 431 - 438, June 2007.

[14] http://www.mathworks.com/products/simpower/blocklist.html

[15] I. Norheim, **"Dynamic Modeling of Turbines (2): Generators, converters, control,"** *Wind Power Conference,* Norway, 6-10 June, 2005.

[16] Chee-Mun Ong, **Dynamic Simulations of Electric Machinery**, Prentice Hall, 1998.

[17] J. R. Espinoza and G. Joos, **"State variable decoupling and power flow control in PWM**

current-source rectifiers," *IEEE Trans. Ind. Electron.*, vol. 45, no. 1, pp. 78–87, Feb. 1998.

[18] T. S. Lee, **"Input-output linearization and zero-dynamics control of three-phase AC/DC voltage-source converters,"** *IEEE Trans. PowerElectron.*, vol. 18, no. 1, pp. 11–22, Jan. 2003.

[19] H. Nikkhajoei and R. Iravani, **"A matrix converter based micro-turbine distributed generation system,"** *IEEE Trans. Power Del*., vol. 20, No. 3, pp. 2182–2192, Jul. 2005.

[20] P. Vas, **Vector control of AC machines**, Clarendon Press, 1994.